Draft version 0.0

ATLAS NOTE

May 6, 2012

Updated search for the Standard Model Higgs boson in the decay channel $H \rightarrow ZZ^{(*)} \rightarrow 4\ell$ with 4.8 fb^{-1} of pp collisions at $\sqrt{s} = 7$ TeV

The ATLAS collaboration

Abstract

Contents

1 Introduction

2 Data and Simulation Samples

The data are subjected to quality requirements: events recorded during periods when the relevant detector components were not operating normally are rejected. The resulting integrated luminosity is 4.81 fb^{-1}, 4.81 fb^{-1} and 4.91 fb^{-1} for the 4μ, $2e2\mu$ and $4e$ final states, respectively.

The $H \to ZZ^{(*)} \to 4\ell$ signal is modelled using the POWHEG Monte Carlo (MC) event generator [**?**, **?**], which calculates separately the gluon-gluon and vector-boson fusion production mechanisms with matrix elements up to next-to-leading order (NLO). The Higgs boson transverse momentum (p_{T}) spectrum in the gluon fusion process is reweighted to match the calculation of Ref. [**?**], which includes quantum chromodynamics (QCD) corrections up to NLO and QCD soft-gluon resummations up to next-to-next-to-leading logarithm (NNLL). POWHEG is interfaced to PYTHIA [**?**] for showering and hadronization, which in turn is interfaced to PHOTOS [**?**] for quantum electrodynamics (QED) radiative corrections in the final state and to TAUOLA [**?**, **?**] for the simulation of τ lepton decays. PYTHIA is used to simulate the production of a Higgs boson in association with a W or a Z boson.

The Higgs boson production cross sections and decay branching ratios [**?**, **?**, **?**, **?**], as well as their uncertainties, are taken from Refs. [**?**, **?**]. The cross sections for the gluon fusion process have been calculated at next-to-leading order (NLO) in QCD [**?**, **?**, **?**], and then at next-to-next-to-leading order (NNLO) [**?**, **?**, **?**]. In addition, QCD soft-gluon resummations up to NNLL are applied for the gluon fusion process [**?**]. The NLO electroweak (EW) corrections are applied [**?**, **?**]. These results are compiled in Refs. [**?**, **?**, **?**] assuming factorisation between QCD and EW corrections. The cross sections for the vector-boson fusion process are calculated with full NLO QCD and EW corrections [**?**, **?**, **?**], and approximate NNLO QCD corrections are available [**?**]. The associated productions with a W or Z boson are calculated at NLO [**?**] and at NNLO [**?**] in QCD, and NLO EW radiative corrections [**?**] are applied. The uncertainty in the production cross section due to the choice of QCD scale is $^{+12}_{-8}\%$ for the gluon fusion process, and $\pm 1\%$ for the vector-boson fusion, associated WH production, and associated ZH production processes [**?**]. The uncertainty in the production cross section due to the parton distribution function (PDF) and α_s is $\pm 8\%$ for gluon-initiated process and $\pm 4\%$ for quark-initiated processes [**?**, **?**, **?**, **?**, **?**]. The Higgs boson decay branching ratio to the four-lepton final state is predicted by PROPHECY4F [**?**, **?**], which includes the complete NLO QCD+EW corrections, interference effects between identical final-state fermions, and leading two-loop heavy Higgs boson corrections to the four-fermion width. Table 1 gives the production cross sections and branching ratios for $H \to ZZ^{(*)} \to 4\ell$ for several Higgs boson masses.

The cross section calculations do not take into account the width of the Higgs boson, which is implemented through a relativistic Breit-Wigner line shape applied at the event-generator level. It has been suggested [**?**, **?**, **?**, **?**] that effects related to off-shell Higgs boson production and interference with other SM processes may become sizeable for the highest masses ($m_H > 400$ GeV) considered in this search. In the absence of a full calculation, a conservative estimate of the possible size of such effects is included as a signal normalization systematic uncertainty following a parameterization as a function of m_H: $150\% \times m_H^3[\mathrm{TeV}]$, for $m_H \geq 300$ GeV [**?**].

The $ZZ^{(*)}$ continuum background is modelled using PYTHIA. The MCFM [**?**, **?**] prediction, including both quark-antiquark annihilation and gluon fusion at QCD NLO, is used for the inclusive total cross section and the shape of the invariant mass of the $ZZ^{(*)}$ system ($m_{ZZ^{(*)}}$). The QCD scale uncertainty has a $\pm 5\%$ effect on the expected $ZZ^{(*)}$ background, and the effect due to the PDF and α_s uncertainties is $\pm 4\%$ ($\pm 8\%$) for quark-initiated (gluon-initiated) processes. An additional theoretical uncertainty of $\pm 10\%$ on the inclusive $ZZ^{(*)}$ cross section is conservatively included due to the missing higher-order QCD corrections for the gluon-initiated process, and a correlated uncertainty on the predicted $m_{ZZ^{(*)}}$ spectrum is estimated by varying the gluon-initiated contribution by 100% [**?**].

The $Z+$jets production is modelled using ALPGEN [**?**] and is divided into two sources: $Z+$light jets

Table 1: Higgs boson production cross sections for gluon fusion, vector-boson fusion and associated production with a W or Z boson in pp collisions at $\sqrt{s} = 7\,\text{TeV}$ [**?**]. The quoted uncertainties correspond to the total theoretical systematic uncertainty. The production cross section for associated production with a W or Z boson is negligibly small for $m_H > 300$ GeV. The decay branching ratio for $H \to 4\ell$, with $\ell = e$ or μ, is reported in the last column [**?**].

m_H [GeV]	$\sigma(gg \to H)$ [pb]	$\sigma(qq' \to Hqq')$ [pb]	$\sigma(q\bar{q} \to WH)$ [pb]	$\sigma(q\bar{q} \to ZH)$ [pb]	$\text{BR}\left(H \to ZZ^{(*)} \to 4\ell\right)$ $[10^{-3}]$
130	$14.1^{+2.7}_{-2.1}$	$1.154^{+0.032}_{-0.027}$	0.501 ± 0.020	0.278 ± 0.014	0.19
150	$10.5^{+2.0}_{-1.6}$	$0.962^{+0.028}_{-0.021}$	0.300 ± 0.012	0.171 ± 0.009	0.38
200	$5.2^{+0.9}_{-0.8}$	$0.637^{+0.022}_{-0.015}$	0.103 ± 0.005	0.061 ± 0.004	1.15
400	2.0 ± 0.3	$0.162^{+0.010}_{-0.005}$	–	–	1.21
600	0.33 ± 0.06	$0.058^{+0.005}_{-0.002}$	–	–	1.23

— which includes $Zc\bar{c}$ in the massless c-quark approximation and $Zb\bar{b}$ from parton showers — and $Zb\bar{b}$ using matrix element calculations that take into account the b-quark mass. The MLM [**?**] matching scheme is used to remove any double counting of identical jets produced via the matrix element calculation and the parton shower, but this scheme is not implemented for b-jets. Therefore, $b\bar{b}$ pairs with separation $\Delta R = \sqrt{(\Delta\phi)^2 + (\Delta\eta)^2} > 0.4$ between the b-quarks are taken from the matrix-element calculation, whereas for $\Delta R < 0.4$ the parton-shower $b\bar{b}$ pairs are used. In this search the $Z+$jets background is normalized using control samples from data. For comparisons with simulation, the QCD NNLO FEWZ [**?**, **?**] and MCFM cross section calculations are used for inclusive Z boson and $Zb\bar{b}$ production, respectively. The $t\bar{t}$ background is modelled using MC@NLO [**?**] and is normalized to the approximate NNLO cross section calculated using HATHOR [**?**]. The effect of the QCD scale uncertainty on the cross section is $^{+4}_{-9}\%$, while the effect of PDF and α_s uncertainties is $\pm 7\%$. Both ALPGEN and MC@NLO are interfaced to HERWIG [**?**] for parton shower hadronization and to JIMMY [**?**] for the underlying event simulation.

Generated events are fully simulated using the ATLAS detector simulation [**?**] within the GEANT4 framework [**?**]. Additional pp interactions in the same and nearby bunch crossings (pile-up) are included in the simulation. The MC samples are reweighted to reproduce the observed distribution of the mean number of interactions per bunch crossing in the data.

3 Lepton Reconstruction and Identification

4 Event Selection Optimization

Contact : F. Cerutti

The kinematic cuts applied at selection level have been otimized aiming at the maximal signal sensitivity. The focus has been on the low mass region, between 120 and 130 GeV where the analysis is more challenging and the differences in kinematics between the signal and the reducible background are larger.

4.1 Optimization for the four muons final state

The optimization procedure is based on a scan of the 6 main kinematic selection variables: M_{12} the opposite-charge di-muon mass coser to the Z one, M_{34} the other opposite-charge di-muons invariant mass, and the transverse momenta of the four leading muons P_{ti} with i ordered from 1 to 4 from the leading to the lowest transverse momentum muon. The position of the cut is chosen at the value that gives the maximum signal sensitivity at a given signal mass. Since the variables are correlated the otpimization procedure was performed in an iterative way looking for minima in the 6 dimentional variable space. The statistical variable used is the probability that the observed number of events, assumed to be equal to the sum of the expected background and signal events in a 6 GeV mass window around the signal mass, is as large or larger than the expected background, the expected P_0. This probability is computed on the basis of a 125 GeV Higgs signal and background events predicted by the MC assuming an integrated luminosity of 20 fb^{-1} at a centre-of-mass energy of 7 TeV. Two methods are used to compute the expected P_0: one is based on the χ^2 asymptotic approximation with the formula described below in Equation 1. In this case the probaility is expressed as the equivalent number of standard deviations Z_0 for a Gaussian probability density function.

$$Z_0 = \sqrt{2\Big((s+b)\ln(1+\frac{s}{b}) - s\Big)} \tag{1}$$

where s and b are the number of signal and background events, respectively.

The second one is based on a simple Poisson marginal probability integral with a linear extrapolation between the two closest integers to the expected signal plus background number of events. Both approach give consistent results in terms of the optimal cuts choice.

In the kinematic optimization for the four muon channel the background estimates are taken form the MC (mc11c samples). This is possible since the reducible background is negligible with respect to the irreducible one and therefore the optimizatin procedure is quite insensitive to its systematics. All kind of backgrounds described Section 2 are taken into account in this procedure. No pileup reweighting and efficiency scale factors are applied in this study. Theirs impact on the optimal cut choice is expected to be negligible for the four muon channel.

In this optimization procedure some constraints were applied to take into account trigger requirements and the fact that some of the background samples are produced with kinematic cuts at gerator level so it does not make sense to explore kinematics too close to these cuts. The most sensitive variables for the optimization are found to be M_{12} and P_{t4}, the lowest transverse momentum of the quadruplet. This is shown in Figure 1 and Figure 2 whether the local expected Z_0 is shown for the 4 muon channels as a function of different kinematic variables. The other variables have a less strong dependency. In particular P_{t1} and P_{t3} have a quite flat behavior so it has been decided to tighten the latter to 10 GeV with respect to the 7 GeV of the previously pubished analysis. Also the cut on M_{34} variable has been tighten with respect to the published analysis with a small increase in the expected Z_0. In general if a small dependency of the expected Z_0 is observed the choice has been to move the cut at the more conservetive value with respect to the redicuble background contribution. The choice of the cuts based on this optimization procedure are summarized in Table 2.

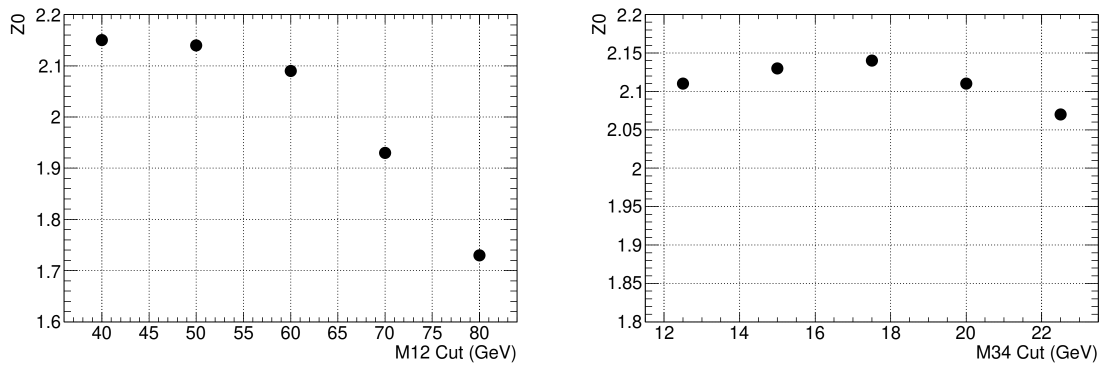

Figure 1: Dependency of the expected Z_0 as described in the text on the mass of the leading pair (left) and of the sub-leading pair (right). The probability refers to a 125 GeV Higgs signal and to an integrated luminosity of 20 fb^{-1} at a cetre-of-mass energy of 7 TeV.

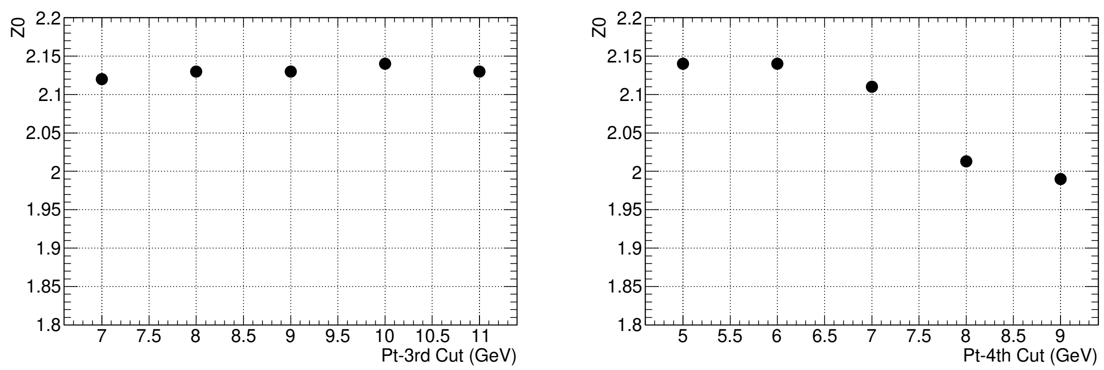

Figure 2: Dependency of the expected Z_0 as described in the text on the mass of the leading pair. (right) dependendy of expected Z_0 as described in the text on the transverse momenta of the third and fourth muons in the quadruplet. The probability refers to a 125 GeV Higgs signal and to an integrated luminosity of 20 fb^{-1} at a cetre-of-mass energy of 7 TeV.

In addition the impact of extending the muon acceptance by adding the SA and Calo-Tag muons as defined in Section 3 has been investigated. The SA muons largely improves the efficiency in the region at large pseudo-rapidities ($2.5 < |\eta| < 2.7$), where the Inner Detector tracking efficiency drops rapidely, and the Calo-Tag muons in the pseudo-rapidity region $|\eta| < 0.1$ where there are not instrumented regions of the Muon Spectrometer due to the passage of ATLAS services. By adding the SA and Calo-Tag muon the signal efficiency, for a 125 GeV Higgs mass, is improved by about 7% in the otpimized kinematic region. The details on the change of the selection, with respect to the published one, and the expected signal significance are reported in Table 3 for an integrated luminosity of 20 fb^{-1} at a centre-of-mass energy of 7 TeV for the four-muons channel alone and a Higgs signal with a mass of 125 GeV.

Usign the same statistical method the impact of other muon selection variables on signal sensitivity was investigated. In particular the use of the calorimetric isolation with pileup corrections was showing a decrease of sensitivity due to the increase of the reducible background. In this case it has been decided to use the uncorrected calorimetric isolation that gives not only better sensitivity but also a sizable reduction of the reducible background (conservative approach). Similar study confirmed the improvement in

Variable	Optimal Cut	Published cut
M_{12}	50 GeV	15 GeV around Z mass
M_{34}	20 GeV	17.5 GeV
P_{t1}	20 GeV	20 GeV
P_{t2}	15 GeV	20 GeV
P_{t3}	10 GeV	7 GeV
P_{t4}	6 GeV	7 GeV

Table 2: Value of optimal cut position for a 125 GeV Higgs mass signal obtained form the procedure described in the text for the four muon final state. The M_{34} cut values refers to a $M_{4\mu}$ mass of 125 GeV.

Selection	Signal	Irreduc. bkg.	Reduc. bkg.	Z_0 Gauss. σ
Published without SA and calo-tag μ	2.25	1.26	0.08	1.64
Published with SA and calo-tag μ	2.40	1.37	0.10	1.69
Optimized with SA and calo-tag μ	3.66	1.92	0.20	2.14

Table 3: Number of signal and background events for the different selections from simulation assuming an integrated luminosity of 20 fb^{-1} at a centre-of-mass energy of 7 TeV for the four-muons channel alone and a Higgs signal with a mass of 125 GeV. No errors on the estimated background is considered here. In the last column the expected local signal significnace, P_0, expressed in terms of equivalent one-sided Gaussian sigma is reported.

sensitivity if the impact parameter significance cut is applied to all four muons of the quadruplet.

4.2 Optimization for channels with Electrons

Due to the different background composition a separate optimization study was performed for channels with sub-leading electrons final states, i.e. the $4e$ and $2\mu 2e$ channels. The kinematic cuts in the quadruplet selection were studied in details after fixing the minimum transverse momentum $P_{te} > 7$ GeV. As in the previous subsection, the main variables studied were the closest mass to the Z one, M_{12}, the lowest momentum of the electrons in the first pair, $P_{t(1,2)}$, and the transverse momentum of the lower energy electrons P_{t3}, while keeping the electron with the lowest momentum $P_{t4} > 7$ GeV. The optimization strategy was to focus on the low-mass Higgs region where potential changes in the kinematic cuts can impact both the signal and reducible backgrounds.

The observables used to quantify the acceptance to MC signal and background events of a given set of cuts are the expected number of events for the integrated luminosity of 2011 (4.8 fb^{-1}) and the global and local significances estimated with Eq. (1). While the global significance looks at a wide range of Higgs mass values (100-180 GeV), the local significance is computed in a limited range of ± 6 GeV (corresponding roughly to 2$\times$FWHM of the experimental resolution) centered on a given Higgs mass hypothesis. The optimization procedure, in parallel with the muon-based procedure, was to re-run the standard analysis with fixed electron and muon identification and isolation event selections on signal and background MC, while varying the targeted variables. Note that the reduction in Z+jets backgrounds is accounted for with the implementation of the new *Eratio* cut for low energy electrons with $P_{te} < 10$ GeV. See Section Section 3 for more details.

Figure 3 shows the expected number of events (left), the global (center) and Local (right) significances as a function of the different kinematic cuts for an integrated luminosity of 4.8 fb^{-1}. The top row of Figure 3 refers to the M_{12}, the middle to the P_{t1} abd the bottom to the P_{t3} kinematic variables respectively.

Figure 3 top clearly show that lowering the value of M_{12} with respect to the published analysis increases the acceptance of the analysis to both signal and background events. Passed the lower bound of $M_{12} > 50$ GeV, the local and global significances reach a stable value where no more significant improvement is possible. For this cut value, the increase in the expected number of events is nearly $\sim$70% for a Higgs signal at 120 GeV.

Figure 3 middle show that lowering the sub-leading P_{t2} gives a small improvement on the significances. If it is lowered to 15 GeV, with respect to the previous value of 20 GeV, the gain in the global significance is at the level of $\sim 4\%$ although the number of Zbb+jets events have increased for a 120-GeV Higgs.

Figure 3 bottom show that further improvement can be reached by increasing the minimum P_t of the third lepton to 10-12 GeV, with respect to the default lowest $P_{te} > 7$ GeV due to a better rejection of Z+jets and $t\bar{t}$ backgrounds characterized by the negative differences in the number of events in Figure Figure 4.2.

In light of the previous one-dimensional kinematic cut parameter scans, it appears reasonable given the increases in the number of events and both local and global significances to improve the analysis sensitivity at low Higgs mass with a different set of kinematic cuts compared to the published analysis. The suggested new values for three dominant cuts were found to be $M_{12} > 50$ GeV, $P_{t(2)} > 15$ GeV, and $P_{t3} > 10$ GeV. The latter exact values can be fine-adjusted to make the analysis of all sub-channels consistent without great impact on the figures stated above.

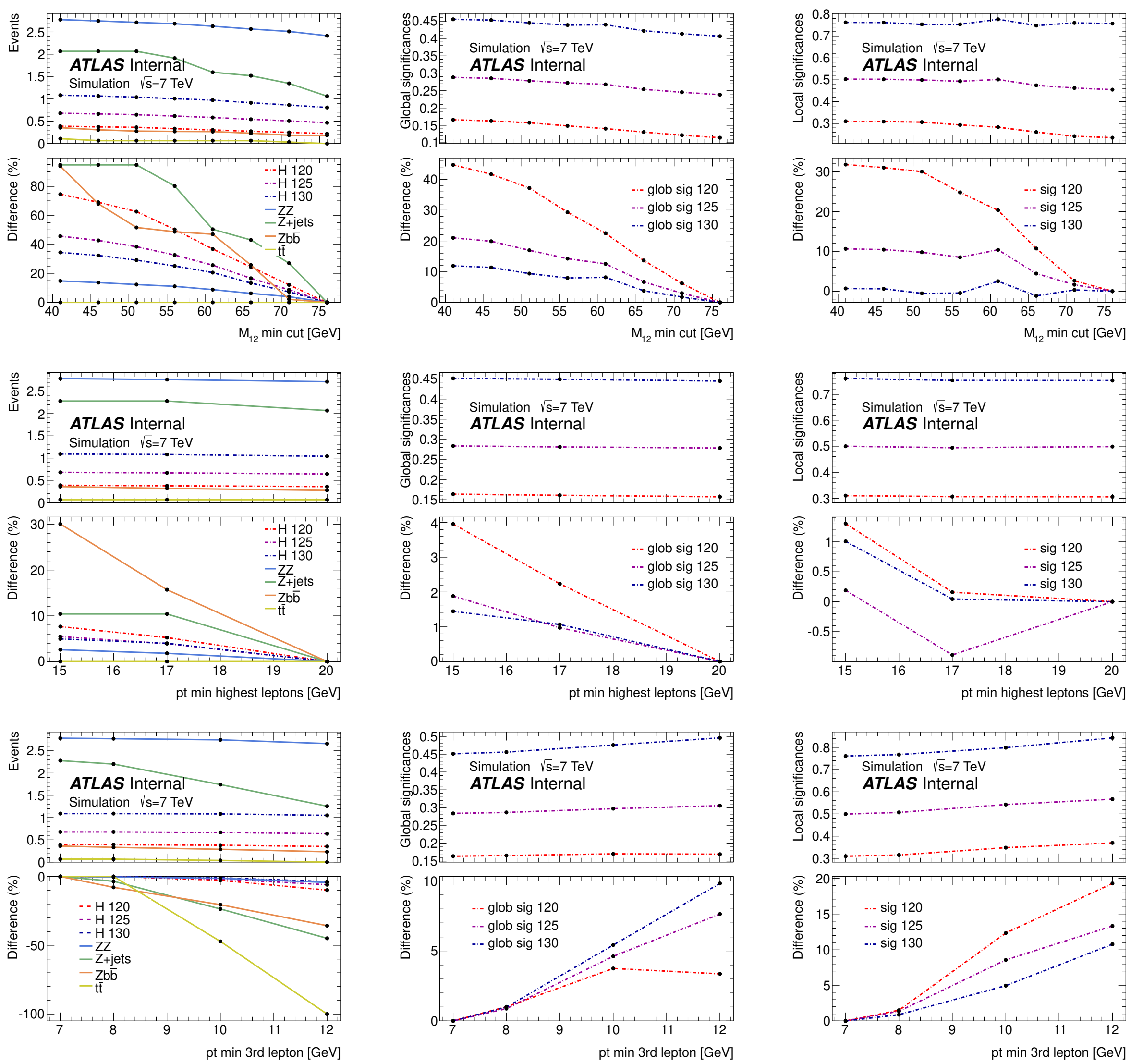

Figure 3: Expected number of events (left) for an integrated luminosity of 4.8fb^{-1}, global (middle) and local (right) significances as a function of the lower bound of M_{12} (top row), the sub-leading P_{t2} found in the first lepton pair (middle row), and the P_{t3} of the third lepton (bottom row). The bottom part of each plot gives the relative difference, in percent, with respect to thepublished analysis.

5 Event Selection

6 Trigger Considerations

Contact : S. Rosati

7 Data based study of the lepton selection criteria

Contact : A. Schaffer

7.1 Efficiency for signal-like leptons

7.1.1 $Z \to ee$

7.1.2 $Z \to \mu\mu$

7.2 Efficiency for background-like leptons

7.2.1 $Z + e$

7.2.2 $Z + \mu$

8 Background Estimation

Contact: C. Anastopoulos

8.1 Data driven cross-checks of the $t\bar{t}$ background

8.2 Estimate of the $Z + \mu\mu$ background

8.2.1 Efficiency estimation for muons in Jets

To estimate the $Z(\rightarrow \mu\mu) + \mu\mu$ background it's important to determine the efficiency of the isolation cuts on muons. To have a sample with more statistics we selected events with a Z that dacays in two muon and an additional muon. The selection of the Z is performed asking two opposite sign combined or tagged muons with $p_{T1} > 20\ GeV$ and $p_{T2} > 10\ GeV$ and an invariant mass $M_Z > 50\ GeV$. The isolation and impactf parameter cuts are the same of the baseline selection. The additional muon could be combined or tagged, standalone or calo. Each of the three categories has its own p_T and η cuts:

- additional combined or tagged muon: $p_T > 5\ GeV$ and $|\eta| < 2.7$
- additional standalone muon: $p_T > 5\ GeV$ and $|\eta| < 2.5$
- additional calo muon: $p_T > 15\ GeV$ and $|\eta| < 0.1$.

The observed number of events and the escpected number of signal and background events for the different MC samples assuming the same integrated luminosity of the data are reported in the table 4. In

Sample	Events with a Z and an additional combined or tagged muon	Events with a Z and an additional standalone muon	Events with a Z and an additional calo muon
Signal $m_H = 130\ GeV$	0.79 ± 0.0094	0.044 ± 0.0022	0.038 ± 0.0020
ZZ	33 ± 0.16	4.2 ± 0.055	2.9 ± 0.046
Zbb	2539 ± 6.9	43 ± 0.89	5.4 ± 0.31
Zjets	7348 ± 66	165 ± 9.9	209 ± 11
$t\bar{T}$	966 ± 5.3	8.4 ± 0.50	3.4 ± 0.32
WZ	195 ± 4.2	9.00 ± 0.89	5.3 ± 0.68
DY	4.3 ± 2.1	0	0
Total BKG	11085 ± 67	230 ± 10	226 ± 11
Data	12888 ± 114	230 ± 15	172 ± 13

Table 4: Observed number of events and escpected number of signal and background events for the different MC samples assuming the same integrated luminosity of the data.

figure 4 the reconstructed invariant mass of the Z is shown both for MC and data for the case of events with a Z and an additional combined or tagged muon. In the left plot the MC distributions are weighted by the cross sections and normalized to the data luminosity. In the right plot the distributions of the reconstructed invariant mass of the Z for MC and data are normalized to 1. The shape of the dstributions are well described by the MC and the normalization agreement in terms of number of events is better then 15% when the third muon is combined or tagged and even better in the other two cases. To estimate the rejection power of the calorimetric isolation a cut on the transverse energy inside a cone with an opening angle of 0.20 around the additional muon divided by its transverse momentum have been applied. The distributions of the calorimetric isolation variable $E_{Tcone20}/p_T$ for the additional muon are shown in figures 9 for the case of a combined or tagged muon (left plot) and standalone (right plot) and in figure 10 for the calo muon (left plot). The number of events with $E_{Tcone20}/p_T < 0.3$, the efficiency and the rejection of this cut are listed in table 5 for all the three cases. The normalization agreement

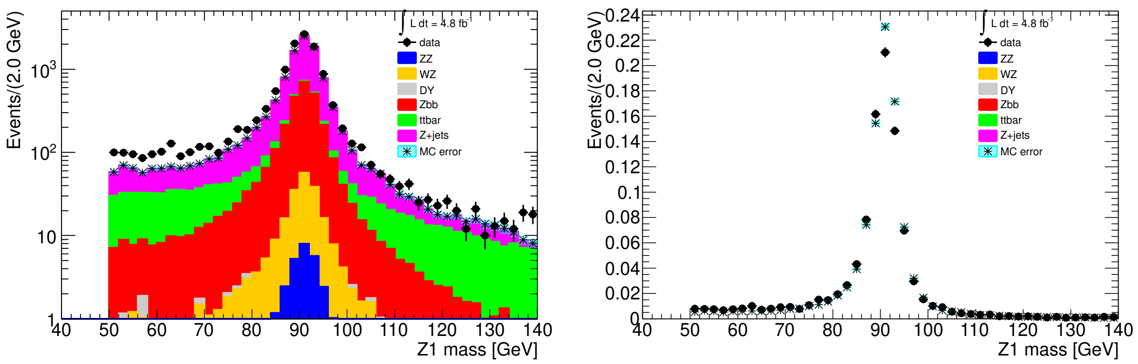

Figure 4: Reconstructed invariant mass of the Z both for MC and data for the case of events with a Z and an additional combined or tagged muon. In the left plot the MC distributions are weighted by the cross sections and normalized to the data luminosity. In the right plot the same distributions are normalized to 1.

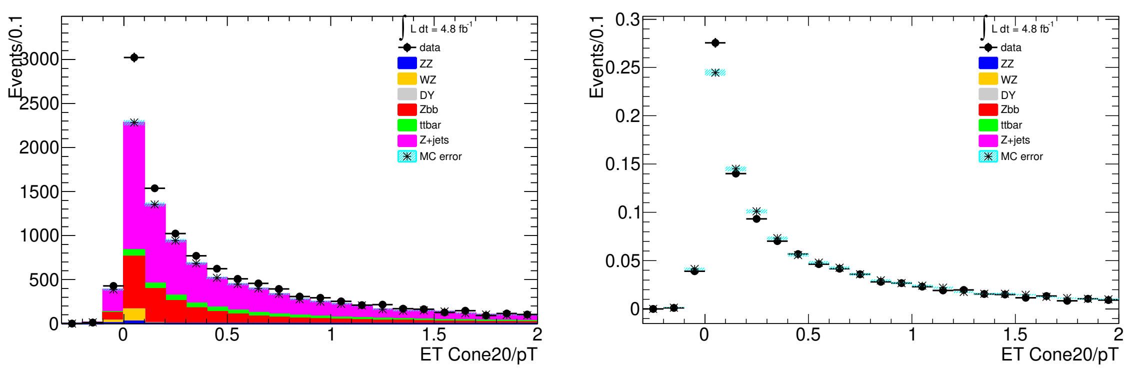

Figure 5: Distributions of the calorimetric isolation variable $E_{Tcone20}/p_T$ for the additional muon in the case of a combined or tagged muon when MC distributions are normalized with cross section (left plot) and when MC and data are normalized to 1 (right plot).

is lways better then the 17% while the efficiency/rejection for MC and data is always compatible. To estimate the rejection power of the track isolation a cut on the transverse momentum inside a cone with an opening angle of 0.20 around the additional muon divided by its transverse momentum have been applied. The distributions of the track isolation variable $p_{Tcone20}/p_T$ for the additional muon are shown in figure 11 for the case of a combined or tagged muon (right plot) and in figures 11 for the case of a calo muon (left plot). The number of events with $E_{Tcone20}/p_T < 0.15$, the efficiency and the rejection of this cut are listed in table 5 for all the three cases. The normalization agreement is always better then the 17% while the efficiency/rejection for MC and data is always compatible.

8.3 Estimate of the $Z + ee$ background

8.4 Data driven cross-checks of the QCD background

8.5 Background shapes

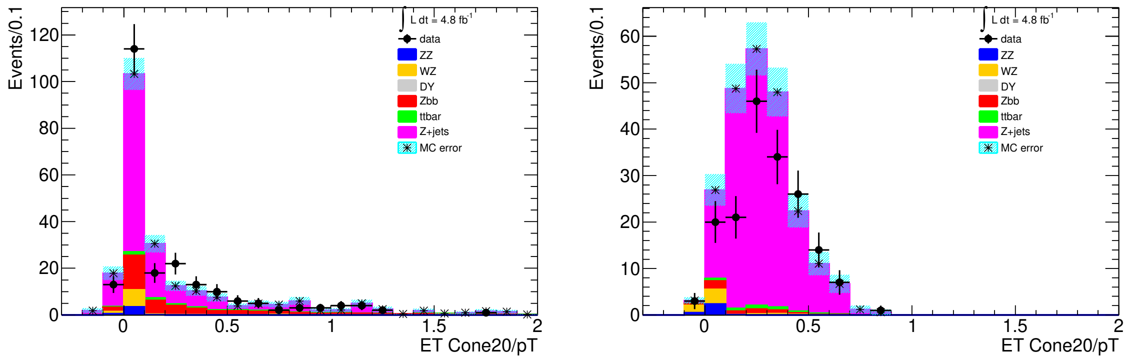

Figure 6: Distributions of the calorimetric isolation variable $E_{Tcone20}/p_T$ for the additional muon in the case of a standalone (left plot) and a calo muon (right plot).

Sample	Events with a Z and an additional combined or tagged muon			Events with a Z and an additional standalone muon			Events with a Z and an additional calo muon		
Signal $m_H = 130$ GeV	0.770 ± 0.009	97 ± 19	3.1 ± 3.4	0.043 ± 0.002	97 ± 71	2 ± 10	0.037 ± 0.002	99 ± 62	2 ± 7
ZZ	32 ± 0.15	97.9 ± 2.5	2.1 ± 0.4	4.11 ± 0.05	99 ± 5	1.2 ± 0.6	2.87 ± 0.05	99 ± 4	0.6 ± 0.3
Zbb	1331 ± 5	52.4 ± 0.7	47.6 ± 0.7	26.7 ± 0.7	62 ± 6	38 ± 5	4.0 ± 0.3	74 ± 16	26 ± 10
Zjets	3232 ± 44	44.0 ± 0.4	56.0 ± 0.4	123.4 ± 9	75 ± 3	25 ± 2	122 ± 8	58 ± 3	42 ± 2
$t\bar{T}$	208 ± 3	21.5 ± 0.6	78.5 ± 1.2	3.4 ± 0.3	41 ± 11	59 ± 13	2.1 ± 0.2	61 ± 21	39 ± 17
WZ	173 ± 4	88.3 ± 2.2	11.7 ± 0.8	8.4 ± 0.9	93 ± 8	7 ± 2	4.9 ± 0.7	93 ± 10	7 ± 3
DY	4.3 ± 2.1			0		0			
Total BKG	4980 ± 44	44.9 ± 0.3	55.1 ± 0.4	166 ± 9	72 ± 3	28 ± 2	136 ± 9	60 ± 3	40 ± 2
Data	6025 ± 78	46.7 ± 0.3	55.3 ± 0.3	167 ± 13	73 ± 3	27 ± 2	90 ± 9	52 ± 3	48 ± 3

Table 5: Observed number of events and escpected number of signal and background events for the different MC samples assuming the same integrated luminosity of the data requiring $E_{Tcone20}/p_T < 0.3$.

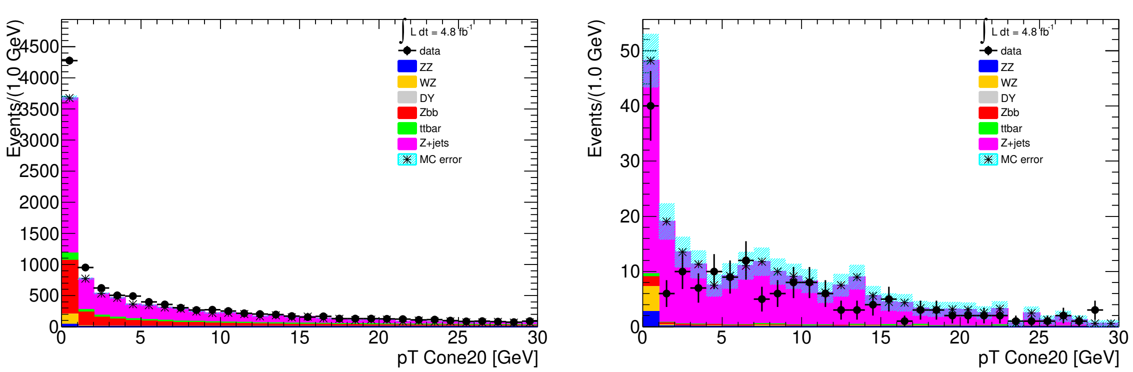

Figure 7: Distribution of the track isolation variable $p_{Tcone20}$ for the additional muon in the case of a combined or tagged additional muon (left plot) and a calo additional muon (right plot).

Sample	Events with a Z and an additional combined or tagged muon			Events with a Z and an additional calo muon		
Signal $m_H = 130$ GeV	0.770 ± 0.009	97 ± 19	3.1 ± 3.4	0.043 ± 0.002	97 ± 71	2 ± 10
0.037 ± 0.002	99 ± 62	2 ± 7				
ZZ	32 ± 0.15	97.9 ± 2.5	2.1 ± 0.4	4.11 ± 0.05	99 ± 5	1.2 ± 0.6
2.87 ± 0.05	99 ± 4	0.6 ± 0.3				
Zbb	1331 ± 5	52.4 ± 0.7	47.6 ± 0.7	26.7 ± 0.7	62 ± 6	38 ± 5
4.0 ± 0.3	74 ± 16	26 ± 10				
Zjets	3232 ± 44	44.0 ± 0.4	56.0 ± 0.4	123.4 ± 9	75 ± 3	25 ± 2
122 ± 8	58 ± 3	42 ± 2				
$t\bar{T}$	208 ± 3	21.5 ± 0.6	78.5 ± 1.2	3.4 ± 0.3	41 ± 11	59 ± 13
2.1 ± 0.2	61 ± 21	39 ± 17				
WZ	173 ± 4	88.3 ± 2.2	11.7 ± 0.8	8.4 ± 0.9	93 ± 8	7 ± 2
4.9 ± 0.7	93 ± 10	7 ± 3				
DY	4.3 ± 2.1			0		0
Total BKG	4980 ± 44	44.9 ± 0.3	55.1 ± 0.4	166 ± 9	72 ± 3	28 ± 2
136 ± 9	60 ± 3	40 ± 2				
Data	6025 ± 78	46.7 ± 0.3	55.3 ± 0.3	167 ± 13	73 ± 3	27 ± 2
90 ± 9	52 ± 3	48 ± 3				

Table 6: Observed number of events and escpected number of signal and background events for the different MC samples assuming the same integrated luminosity of the data requiring $E_{Tcone20}/p_T < 0.3$.

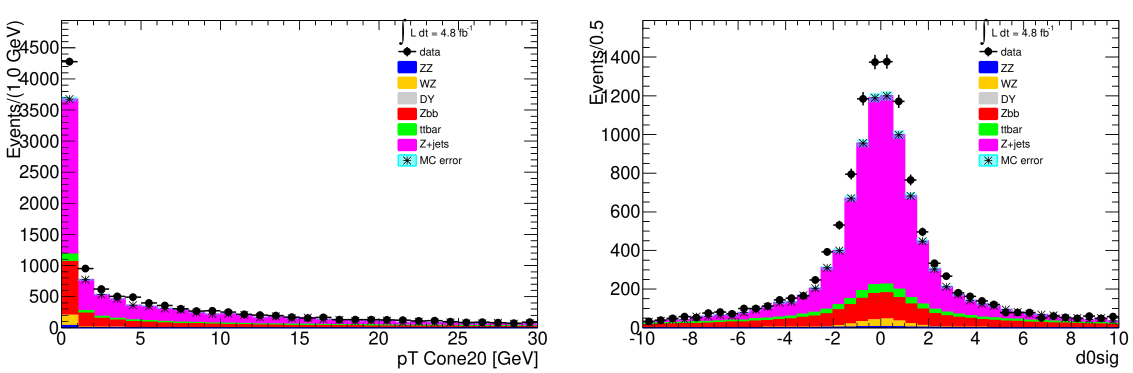

Figure 8: Z mass; iso

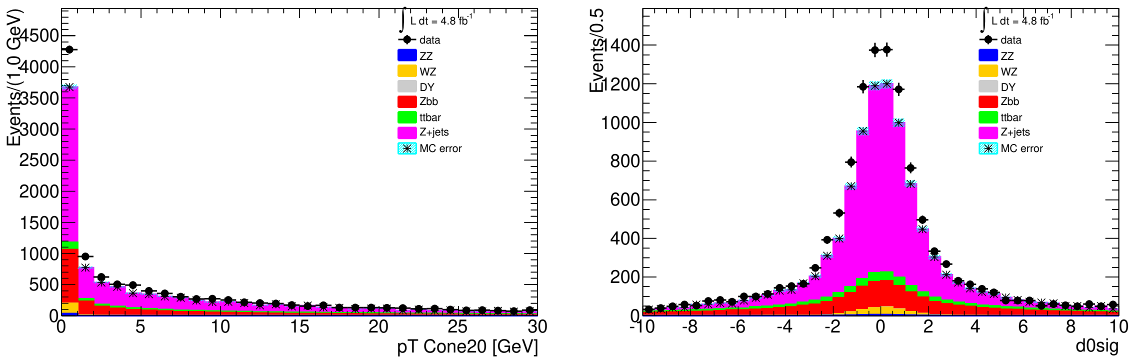

Figure 9: Z mass; iso

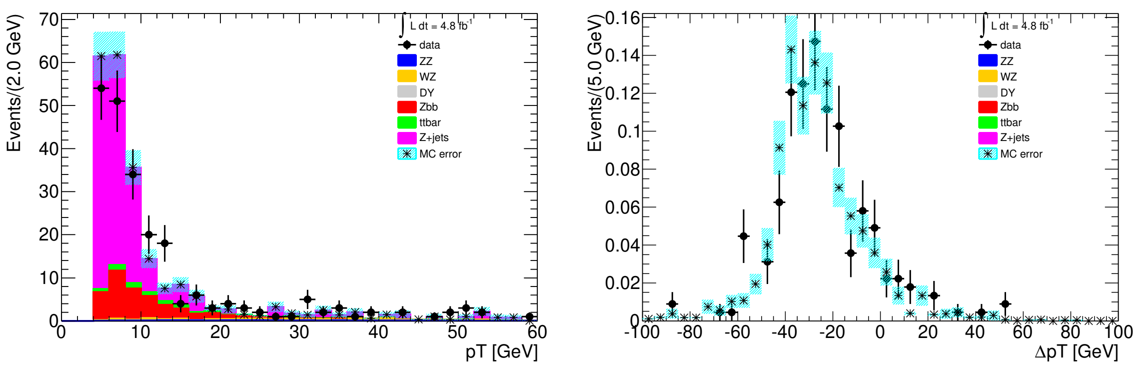

Figure 10: Z mass; iso

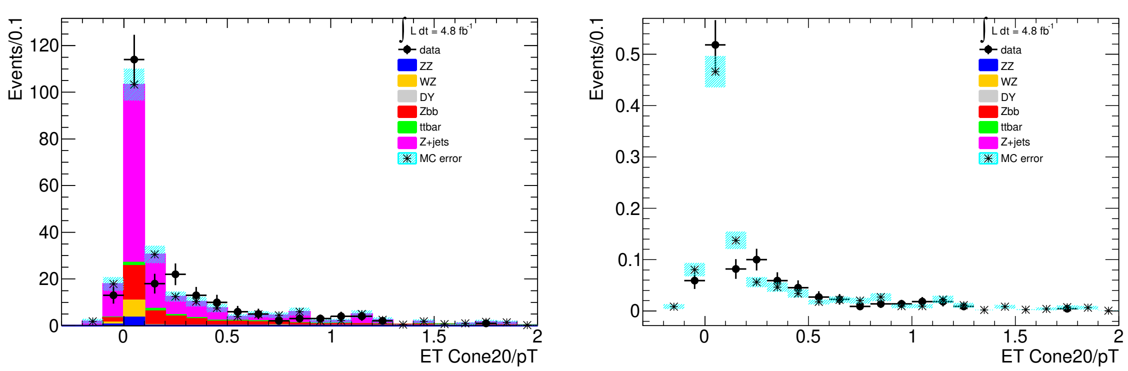

Figure 11: Z mass; iso

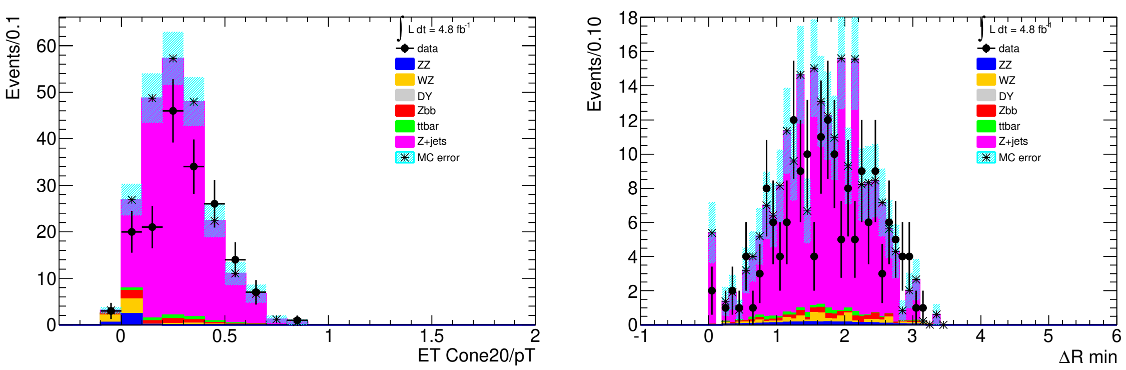

Figure 12: Z mass; iso

9 Results of Event Selection

10 Systematic Uncertainties

Contact : J. Hoffman

11 Exlusion limits and p-values

Contact : L. Flores

12 Conclusions

Appendices